PROCEEDINGS, 45th Workshop on Geothermal Reservoir Engineering
Stanford University, Stanford, California, February 10-12, 2020
SGP-TR-216

Anisotropic Elastic Properties of the First EGS Collab Testbed Revealed from the Campaign Cross-Borehole Seismic Data

Kai Gao[1], Lianjie Huang[1], Hunter A. Knox[2], Paul C. Schwering[3], Charles R. Hoots[3], Jonathan Ajo-Franklin[4], Timothy Kneafsey[5], and EGS Collab Team[6]

[1]Los Alamos National Laboratory, Los Alamos, NM 87545, USA; [2] Pacific Northwest National Laboratory, Richland, WA 99352, USA; [3]Sandia National Laboratories, Albuquerque, NM 87123, USA; [4]Rice University, Houston, TX 77005, USA; [5]Lawrence Berkeley National Laboratory, Berkeley, CA 94720, USA; EGS Collab Team (see the footnote[6])

kaigao@lanl.gov; ljh@lanl.gov

Keywords: Enhanced Geothermal System, anisotropy, fracture, anisotropic traveltime tomography, elastic-waveform inversion

ABSTRACT

Accurate characterization of reservoir rocks is crucial for fracture stimulations and time-lapse reservoir monitoring in enhanced geothermal systems. Campaign cross-borehole seismic data were collected as part of a comprehensive characterization suite of the first EGS Collab testbed prior to EGS Collab hydraulic stimulation experiments. The testbed was established in metamorphic, crystalline rock at the 4850 ft deep at the Sanford Underground Research Facility in Lead, South Dakota. Previous anisotropic traveltime tomography results revealed a heterogeneous velocity structure and strong anisotropy with features trending in a primarily northwest/southeast orientation. Based on these results, we employ an anisotropic elastic-waveform inversion method to further refine structures and rock properties within the first EGS Collab testbed. This method uses seismic waveform data, which in principle is capable of revealing higher-resolution and more accurate rock properties compared with traveltime tomography. We obtain a set of high-resolution P-/S-wave velocity and Thomsen anisotropic parameter models, and compare them with the traveltime tomography models. We focus on the portion of the testbed relevant to the hydraulic stimulation and flow experiments, which were performed subsequent to the campaign cross-borehole seismic characterization efforts. Furthermore, we will show that the inverted anisotropic medium parameter models can provide quantitative information on the fracture orientation and density in space, and can serve as important guidance for time-lapse active seismic monitoring during the hydraulic stimulation activities.

1. INTRODUCTION

The Enhanced Geothermal System (EGS) Collab project focuses on understanding and predicting permeability enhancement and evolution in rocks, including how to create sustained and distributed permeability for heat extraction from the reservoir by generating new fractures that complement existing fractures (e.g., Kneafsey et al., 2018). For characterizing the properties of the host rock at the first EGS Collab tested, the project conducted geophysical characterization and monitoring using such as electrical resistivity tomography (Johnson et al., 2019), seismic traveltime tomography (Gao et al., 2019) and elastic-waveform inversion (Chi el al., 2019, 2020). For the seismic characterization, the project acquired campaign cross-borehole seismic data recorded using a 96-channel array of hydrophones, accelerometers, and geophones (Schwering et al., 2018; Linneman et al., 2018).

We develop an anisotropic adjoint-state first-arrival traveltime tomography (AA-FATT) method and an anisotropic elastic-waveform inversion (AEWI) method to characterize anisotropic characteristics of the host rock at the EGS Collab testbed using the campaign cross-borehole seismic data. AA-FATT seeks to match the synthetic first-arrival traveltimes with the observed first-arrival times to invert for a set of best-fit anisotropic models. Different from ray-based traveltime tomography approaches, adjoint-state FATT employs the adjoint-state eikonal equation to facilitate the computation of medium parameter gradients, leading to an efficient whole-space coverage of wavepaths and inverted parameters. AEWI seeks a set of anisotropic elastic parameter models, including P- and S-wave velocities, Thomsen parameters and density, by fitting synthetic seismic waveforms with observed seismic waveforms. Using both phase and amplitude information embedded in seismic waveform data, AEWI usually produces medium parameter models with higher spatial

[6] J. Ajo-Franklin, T. Baumgartner, K. Beckers, D. Blankenship, A. Bonneville, L. Boyd, S. Brown, J.A. Burghardt, C. Chai, Y. Chen, B. Chi, K. Condon, P.J. Cook, D. Crandall, P.F. Dobson, T. Doe, C.A. Doughty, D. Elsworth, J. Feldman, Z. Feng, A. Foris, L.P. Frash, Z. Frone, P. Fu, K. Gao, A. Ghassemi, Y. Guglielmi, B. Haimson, A. Hawkins, J. Heise, M. Horn, R.N. Horne, J. Horner, M. Hu, H. Huang, L. Huang, K.J. Im, M. Ingraham, E. Jafarov, R.S. Jayne, S.E. Johnson, T.C. Johnson, B. Johnston, K. Kim, D.K. King, T. Kneafsey, H. Knox, J. Knox, D. Kumar, M. Lee, K. Li, Z. Li, M. Maceira, P. Mackey, N. Makedonska, E. Mattson, M.W. McClure, J. McLennan, C. Medler, R.J. Mellors, E. Metcalfe, J. Moore, C.E. Morency, J.P. Morris, S. Nakagawa, G. Neupane, G. Newman, A. Nieto, C.M. Oldenburg, T. Paronish, R. Pawar, P. Petrov, B. Pietzyk, R. Podgorney, Y. Polsky, J. Pope, S. Porse, J.C. Primo, C. Reimers, B.Q. Roberts, M. Robertson, W. Roggenthen, J. Rutqvist, D. Rynders, M. Schoenball, P. Schwering, V. Sesetty, C.S. Sherman, A. Singh, M.M. Smith, H. Sone, E.L. Sonnenthal, F.A. Soom, P. Sprinkle, C.E. Strickland, J. Su, D. Templeton, J.N. Thomle, C. Ulrich, N. Uzunlar, A. Vachaparampil, C.A. Valladao, W. Vandermeer, G. Vandine, D. Vardiman, V.R. Vermeul, J.L. Wagoner, H.F. Wang, J. Weers, N. Welch, J. White, M.D. White, P. Winterfeld, T. Wood, S. Workman, H. Wu, Y.S. Wu, E.C. Yildirim, Y. Zhang, Y.Q. Zhang, Q. Zhou, M.D. Zoback

resolution compared with those obtained using FATT approaches. The goal of AA-FATT and AEWI is to provide accurate, reliable and high-resolution medium parameter models for accurate fracture imaging and microseismic event location/focal mechanism inversion, etc.

2. METHODOLOGY

2.1 Adjoint-state anisotropic first-arrival traveltime tomography

AA-FATT uses the traveltime information of seismic arrivals to invert for anisotropic properties of the medium. Our algorithm produces the best-fit anisotropic models by minimizing the observed first-arrival traveltime T_{obs} and the numerical synthetic first-arrival traveltime T_{syn} computed using 3D fully anisotropic eikonal equation:

$$(V_p,\varepsilon,\delta)^* = \arg\min_{V_p,\varepsilon,\delta} \| T_{\text{obs}} - T_{\text{syn}} \|_2^2 , \tag{1}$$

where V_p, ε and δ are the P-wave velocity and Thomsen parameters, respectively. The synthetic data also depend on TTI (transversely isotropy with a tilted symmetry axis) medium symmetry axis tilt angles θ and ϕ, which are fixed during the AA-FATT to reduce inter-parameter crosstalk.

We use the conjugate-gradient inversion framework to update the anisotropic models. We compute the gradients of medium parameters using the adjoint-state eikonal equation. In our algorithm, we solve the following 3D anisotropic eikonal equation to obtain the first-arrival traveltime field associated with the qP-wave mode:

$$v_x^2(\partial_x t)^2 + v_y^2(\partial_y t)^2 + v_z^2(\partial_z t)^2[1-2(\varepsilon-\delta)v_z^2((\partial_x t)^2 + ((\partial_y t)^2)] = 1 , \tag{2}$$

where t is the traveltime field, $v_{x,y,z}$ are the qP-wave velocities along the x-, y- and z-directions, respectively, and ε and δ are Thomsen parameters. We develop a high-order hybrid anisotropic eikonal solver to solve equation (2). The adjoint-state equation associated with equation (2) can be derived using a similar procedure described in bin Waheed et al. (2016).

2.2 Anisotropic elastic-waveform inversion

We further update the anisotropic models using AEWI. AEWI updates elastic anisotropic medium parameter models by minimizing the observed seismic waveform $\mathbf{d}_{\text{obs}}$ and the synthetic waveform $\mathbf{d}_{\text{syn}}$ computed using 3D fully anisotropic elastic-wave equation:

$$(V_p,V_s,\rho,\varepsilon,\delta,\gamma)^* = \arg\min_{V_p,V_s,\rho,\varepsilon,\delta,\gamma} \| \mathbf{d}_{\text{obs}} - \mathbf{d}_{\text{syn}} \|_2^2 , \tag{3}$$

where V_p and V_s are the P- and S-wave velocities of the medium, respectively, ρ is the medium density and ε, δ and γ are Thomsen parameters. The synthetic seismic data also depend on TTI medium's symmetry axis tilt angles θ and ϕ, which are fixed during AEWI to reduce inter-parameter crosstalk artifacts. In AA-FATT, the S-wave velocity V_s and its associated anisotropy indicator parameter γ cannot be inverted because of the non-uniqueness of two split qS-wave modes and low signal-to-noise ratio of qS-wave first arrivals. By contrast, AEWI can update these two parameters in a unified framework. In addition, we can update the density parameter using AEWI, providing more information for rock characterization.

Conventional FWI in the form of equation (2) may encounter cycle-skipping or local minimum issue caused by the complexity of seismic data. To improve inversion convergence, we employ the following misfit function in our AEWI:

$$(V_p,V_s,\rho,\varepsilon,\delta,\gamma)^* = \arg\min_{V_p,V_s,\rho,\varepsilon,\delta,\gamma} \| A_\tau(\mathbf{d}_{\text{obs}},\mathbf{d}_{\text{obs}}) - C_\tau(\mathbf{d}_{\text{obs}},\mathbf{d}_{\text{syn}}) \|_2^2 , \tag{4}$$

where $A_\tau(\mathbf{d}_{\text{obs}},\mathbf{d}_{\text{obs}})$ is the auto-correlation of the observed seismic waveform $\mathbf{d}_{\text{obs}}$ with a time delay of τ, and $C_\tau(\mathbf{d}_{\text{obs}},\mathbf{d}_{\text{syn}})$ is the cross-correlation between the synthetic $\mathbf{d}_{\text{obs}}$ and the observed waveforms $\mathbf{d}_{\text{syn}}$ with a time delay of τ. The gradients of anisotropic elastic parameters can be computed using the adjoint-state method. In our algorithm, we first compute the gradients associated with the elasticity parameters C_{ij} as (Vigh et al., 2014):

$$G_{C_{ij}} = -\int_0^T \frac{\partial \mathbf{C}}{\partial C_{ij}} \frac{\partial \grave{o}}{\partial t} \grave{o}^\dagger dt , \tag{5}$$

with $i,j = 1,2,\cdots$, where $\grave{o}$ and $\grave{o}^\dagger$ are the source and adjoint strain wavefields, respectively. Then we use these gradients to compute the gradients associated with the parameters in equation (4) based on the differentiation chain rule. An AEWI algorithm parameterized using the six velocity-density-Thomsen parameters can be easier to be constrained compared with that parameterized with C_{ij}. For 3D

general anisotropic media, the number of independent C_{ij} can be up to 21, leading to significant difficulties in reducing inter-parameter crosstalk artifacts in inversion results.

3. RESULTS

3.1 Geometry settings and existing results

We show the data acquisition configuration for collecting campaign cross-borehole seismic data in Figure 1a. A total of 63 sources are placed in the injection well. Each common-shot gather contains either 144 or 96 hydrophone receivers in the production well. Each common-shot gather records approximately 0.1 s of seismic waveforms. The data has a wide frequency band ranging from 2 KHz to 12.5 KHz. The signal-to-noise ratio for frequency components below or above this band is low. The region of interest for seismic characterization is approximately 15 m in the x-direction, 75 m in the y-direction and 18 m in the z-direction.

The EGS Collab project produced a P-wave velocity model for this region using isotropic first-arrival traveltime tomography (Figure 1b). The value range of the inverted P-wave velocity model is from approximately 5000 m/s to approximately 6800 m/s. The result shows a velocity variation of approximately 1800 m/s at the end of the injection/production wells away from the collar, within a spatial range of approximately 15 m. Such a velocity change within a small volume of rock may result from the isotropic assumption.

3.2 AA-FATT inversion results

To characterize the region of interest with better petro-physical plausibility, we conduct AA-FATT, to obtain a set of anisotropic parameters for this region.

Starting from a homogeneous P-wave velocity model with a value of 5800 m/s, we first conduct an isotropic adjoint-state FATT. This inverted velocity model has a value range of 4500 to 7800 m/s (Figure 2). This value range is even larger than that in Figure 1b. In addition, we find that there are obvious artifact-like velocity anomalies at the two ends of both injection and production wells, indicating the possibility of a biased inversion result under the assumption of isotropic medium. Our isotropic adjoint-state FATT resembles the issue of drastic velocity variations within small spatial range shown in Figure 1b.

We conduct a second traveltime tomography test assuming VTI (transversely isotropy with a vertical symmetry axis) anisotropy for this region. The initial P-wave velocity model is homogeneous with a value of 5800 m/s, accompanied with homogeneous Thomsen parameter ε and δ models, with values 0.2 and 0.1, respectively. We show the inverted P-wave velocity and two Thomsen parameters using the VTI AA-FATT in Figure 3a, 3b and 3c, respectively. The inverted P-wave velocity values range from 5400 to 5900 m/s, a much smaller variation range compared with that of the isotropic FATT. However, the inverted Thomsen parameter ε and δ models are not consistent with each other. Particularly, the inverted ε model indicates low anisotropy between the injection and production wells, while the inverted δ models has a large value between the injection and production wells, indicating a high level of anisotropy.

We conduct a third AA-FATT test using a HTI (transversely isotropy with a horizontal symmetry axis) medium, and show the results for the inverted P-wave velocity, and Thomsen parameters ε and δ in Figure 4a, 4b and 4c, respectively. In most parts of the region of interest, the P-wave velocity value has a mild spatial variation, except the end of the injection well where the data coverage is poor. The spatial patterns of the two inverted Thomsen parameters are apparently more consistent with each other compared with those of the VTI FATT inversion, indicating a more reasonable anisotropic assumption (HTI) for this region. A potential issue with the HTI FATT inversion result is that the values of the inverted Thomsen parameters can be fairly large in some parts of the model. For example, a value of 0.6 for ε indicates an almost 48% faster vertical qP-wave velocity with respect to the horizontal qP-wave velocity in the HTI medium. It is not yet clear whether such large velocity discrepancy is possible in realistic geology. Therefore, it is necessary to cross-validate the inversion results with those obtained using other geophysical approaches, e.g., electric resistivity tomography.

Figure 5a, 5b and 5c compare the final traveltime misfit measured in millisecond. It is evident that the traveltime misfit in the HTI FATT inverted model is more concentrated around zero compared with those for isotropic FATT and VTI FATT, indicating the HTI medium is closer to real geology compared with the other two. The misfit convergence curves associated with the three FATT inversions shown in Figure 5d also further demonstrate the higher accuracy and reliability of the HTI FATT result compared with those for the other two types of media.

3.3 AEWI inversion results

To improve the spatial resolution of anisotropic elastic models, we conduct AEWI based on the inversion results shown in Figure 4. Our AEWI requires appropriate S-wave velocity and Thomsen anisotropic parameter γ, as well as density ρ, as initial parameter models in addition to the models shown in Figure 4. Since these quantities can be very difficult to obtain using traveltime tomography, we create the density model from the AA-FATT inverted P-wave velocity using Gardner's rule as $\rho = 310 \times V_p^{0.25}$, with unit kg/m^3, and a S-wave velocity model by simple scaling $V_s = V_p / \sqrt{3}$. The Thomsen parameter γ is linearly scaled from the parameter ε.

We show the P-wave velocity, S-wave velocity, Thomsen parameters ε, δ and γ, and density models inverted using our 3D AEWI method in Figures 6a-6f. The inverted model has an evidently improved spatial resolution compared with the FATT inversion results in Figure 5, particularly for the region between the injection and production wells. We find that the spatial pattern of the P-wave velocity model is similar to that of the S-wave velocity model. We observe relative lower velocity values at the two ends of both injection and production wells, while there is a relative high-velocity zone in the central region between the two wells. The three inverted Thomsen parameters

have similar spatial patterns, indicating a relative lower anisotropy zone in the central region between the two wells. Finally, the inverted density models shows mildly lower values in most regions between the two wells.

We further verify the existence of anisotropy from the campaign cross-borehole seismic data. Figure 7a shows an unprocessed common-shot gather in the campaign cross-borehole seismic data. This gather is the pressure component recorded in the production well. To facilitate our AEWI, we process this common-shot gather and show the early arrivals of the shot gather in Figure 7b, where we find that there are S-wave mode in the data with a larger slope (i.e., lower propagation velocity) compared with qP-wave mode first arrivals.

If the medium is isotropic, there should be no S-wave mode (i.e., shear deformation energy) appearing in the pressure component (i.e., normal deformation energy). In contrast, if the medium is anisotropic, then the qS-wave mode contains not only shear deformation, but also normal deformation. In this case, the pressure component contains qS-wave mode leakage, i.e., the normal deformation energy of qS-wave mode. Therefore, the existence of S-wave mode in the pressure component is a clear indication of non-trivial seismic anisotropy. In fact, if we conduct an elastic-wave modeling using only the inverted P- and S-wave velocity models (shown in Figure 7c), we observe that there are absolutely no S-wave mode in the recorded pressure data. By contrast, the synthetic pressure-component data computed using the inverted anisotropic elastic models (shown in Figure 7d) shows clearly leaked qS-wave mode in the data denoted by the red arrows.

We find similar existence of qS-wave mode in the field data for another common-shot gather (Figure 8b) and in the synthetic data computed using the inverted anisotropic elastic model (Figure 8d). The synthetic data computed in isotropic elastic model for this common-shot gather (Figure 8c) lack such an S-wave mode. The consistency between the observed and synthetic pressure-component data on qS-wave mode existence further demonstrates the reliability of our AEWI results and the existence of anisotropy in the host rock for the first EGS Collab testbed.

4. CONCLUSIONS

We have developed a 3D fully anisotropic first-arrival traveltime tomography method and a 3D fully anisotropic elastic-waveform inversion method, and applied the methods to the campaign cross-borehole seismic data acquired at the first EGS Collab testbed. We have conducted a series of anisotropic first-arrival traveltime tomography and anisotropic elastic-waveform inversion tests, and have found that the region between the injection and production wells can be well characterized by a transversely isotropic medium with horizontal symmetry axis. In addition, the anisotropy associated with this HTI medium is fairly strong, indicating the possibility of large amount of pre-existing fractures or finely layered metasedimentary rocks in this region. The existence of strong seismic anisotropy in this region is also supported by the leaked S-wave mode in the pressure-component seismic data.

5. ACKNOWLEDGMENTS

This material was based upon work supported by the U.S. Department of Energy (DOE), Office of Energy Efficiency and Renewable Energy (EERE), Office of Technology Development, Geothermal Technologies Office, under Contract No. 89233218CNA000001 to Los Alamos National Laboratory (LANL) and under Award Number DE-AC02-05CH11231 with Lawrence Berkeley National Laboratory (LBNL). LANL is operated by Triad National Security, LLC, for the National Nuclear Security Administration (NNSA) of U.S. DOE. This research used resources provided by the LANL Institutional Computing Program, which is supported by the U.S. DOE NNSA under Contract No. 89233218CNA000001. The United States Government retains, and the publisher, by accepting the article for publication, acknowledges that the United States Government retains a non-exclusive, paid-up, irrevocable, world-wide license to publish or reproduce the published form of this manuscript, or allow others to do so, for United States Government purposes. The research supporting this work took place in whole or in part at the Sanford Underground Research Facility in Lead, South Dakota. The assistance of the Sanford Underground Research Facility and its personnel in providing physical access and general logistical and technical support is acknowledged. We thank Benxin Chi and Zongcai Feng of LANL for helpful discussions.

REFERENCES

Chi, B., Huang, L., Gao, K., Ajo-Franklin, J., Kneafsey, T.J., and EGS Collab Team, High-Resolution Imaging of Created Fractures in EGS Collab Experiments Using CASSM Data, *Geothermal Resources Council Transactions*, Geothermal Resources Council Annual Meeting, Palm Springs, CA (2019).

Chi, B., Huang, L., Gao, K., Ajo-Franklin, J., Kneafsey, T.J., and EGS Collab Team, Anisotropic Imaging of Created Fractures in EGS Collab Experiments Using CASSM Data, *Proceedings*, 45th Workshop on Geothermal Reservoir Engineering, Stanford University, Stanford, CA (2020).

Gao., K., Huang, L., Knox, H., Schwering, P., Hoots, C., Blankenship, D., Ajo-Franklin, J., Kneafsey, T.J., and EGS Collab Team, Anisotropic Traveltime Tomography of Campaign Cross-Borehole Seismic Data from the First EGS Collab Testbed, *Geothermal Resources Council Transactions*, Geothermal Resources Council Annual Meeting, Palm Springs, CA (2019).

Johnson, T., Strickland, C., Knox, H., Thomle, J., Vermuel, V., Ulrich, C., Kneafsey, T., Blankenship, D., and EGS Collab Team, EGS Collab Project Electrical Resistivity Tomography Characterization and Monitoring Status, *Proceedings*, 44th Workshop on Geothermal Reservoir Engineering, Stanford University, Stanford, CA (2019).

Kneafsey, T.J., Dobson, P., Blankenship, D., Morris, J., Knox, H., Schwering, P., White, M., Doe, T., Roggenthen, W., Mattson, E., Podgorney, R., Johnson, T., Ajo-Franklin, J., Valladao, C., and the EGS Collab team, An Overview of the EGS Collab Project: Field

Validation of Coupled Process Modeling of Fracturing and Fluid Flow at the Sanford Underground Research Facility, Lead, SD, *Proceedings*, 43rd Workshop on Geothermal Reservoir Engineering Stanford University, Stanford, CA (2018).

Linneman, D., Knox, H., Schwering, P., and Hoots, C., The EGS Collab Hydrofracture Experiment at the Sanford Underground Research Facility – Campaign Cross-Borehole Seismic Characterization, *Abstracts*, AGU Fall Meeting, Washington, D.C. (2018).

Schwering, P., Knox, H., Hoots, C., Linneman, D., Ajo-Franklin, J., and EGS Collab Team, The EGS Collab Hydrofracture Experiment at the Sanford Underground Research Facility – Campaign Cross-Borehole Seismic Characterization, *Geothermal Resources Council Transactions*, Geothermal Resources Council Annual Meeting, Reno, NV (2018).

Vigh, D., Jiao, K., Watts, D., and Sun, D.: Elastic full-waveform inversion application using multicomponent measurements of seismic data collection, *Geophysics*, 79, (2014), R63-R77.

bin Waheed, U., Flagg, G., and Yarman, C.E.: First-arrival traveltime tomography for anisotropic media using the adjoint-state method, *Geophysics*, 81, (2016), R147–R155.

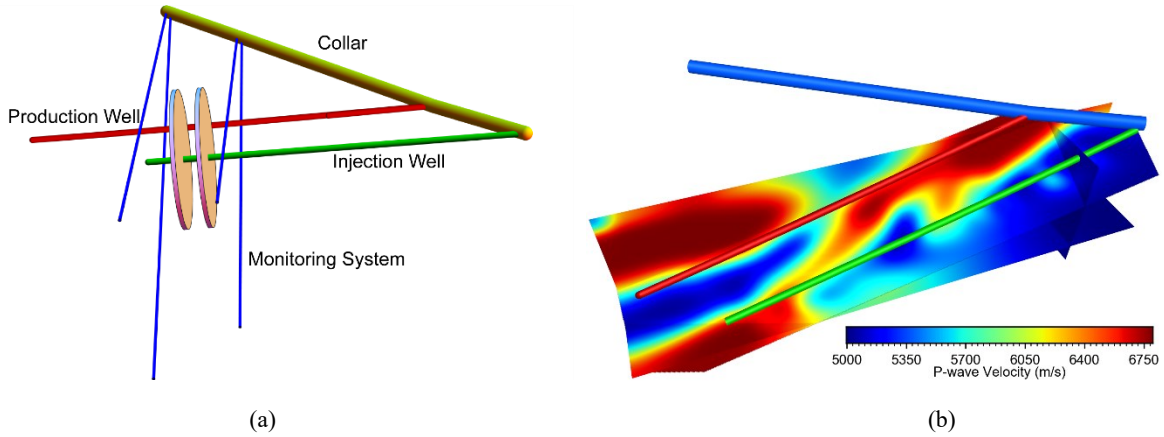

Figure 1: (a) A sketch of the EGS Collab injection-production-monitoring system. (b) P-wave velocity model obtained by SNL/LBNL using traveltime tomography in isotropic media.

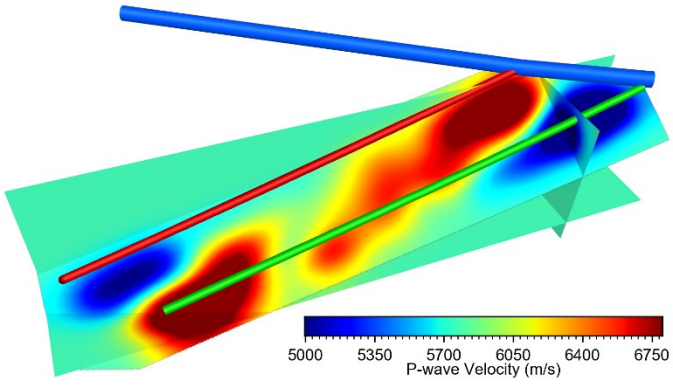

Figure 2: Inverted P-wave velocity obtained using isotropic adjoint-state FATT.

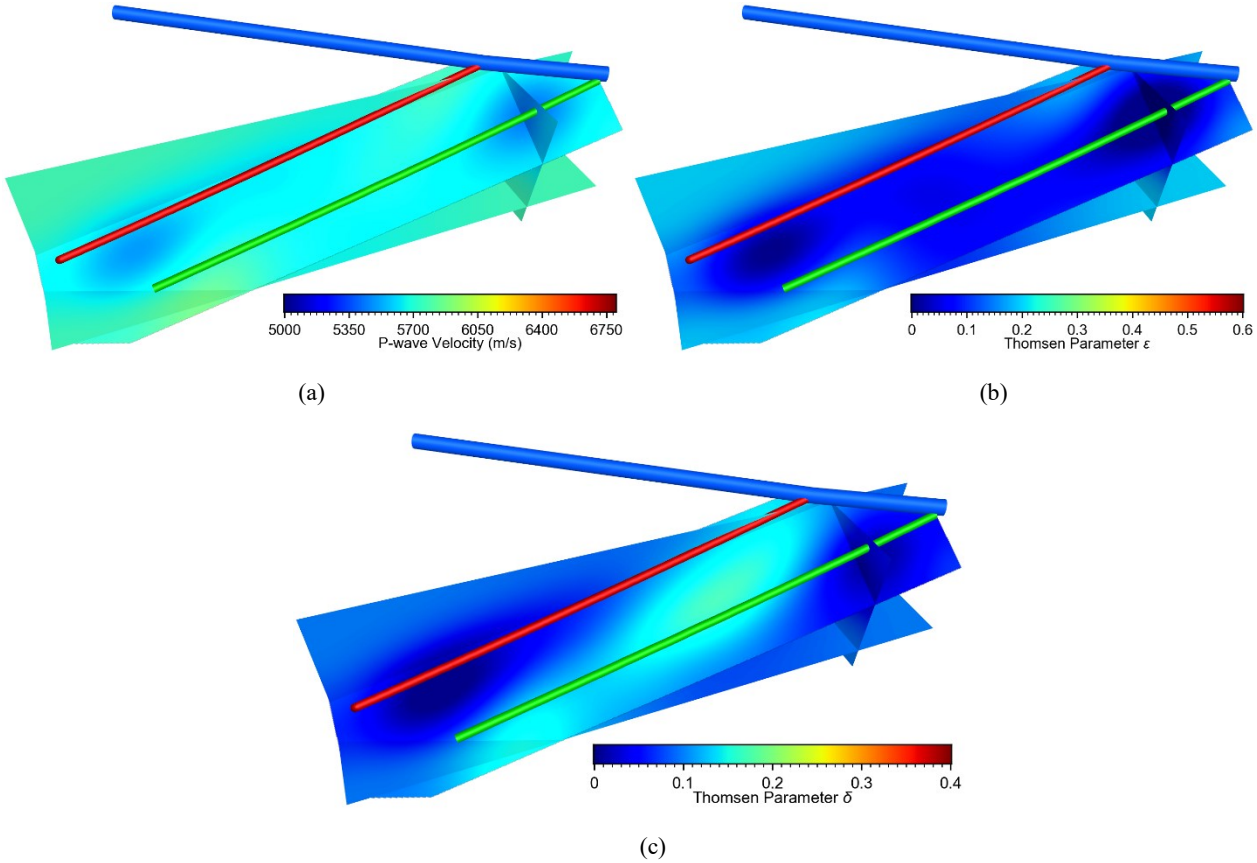

(a) (b)

(c)

Figure 3: Inverted P-wave velocity (a), Thomsen anisotropic parameter ε (b) and Thomsen anisotropic parameter δ (c) obtained using our AA-FATT by assuming VTI medium.

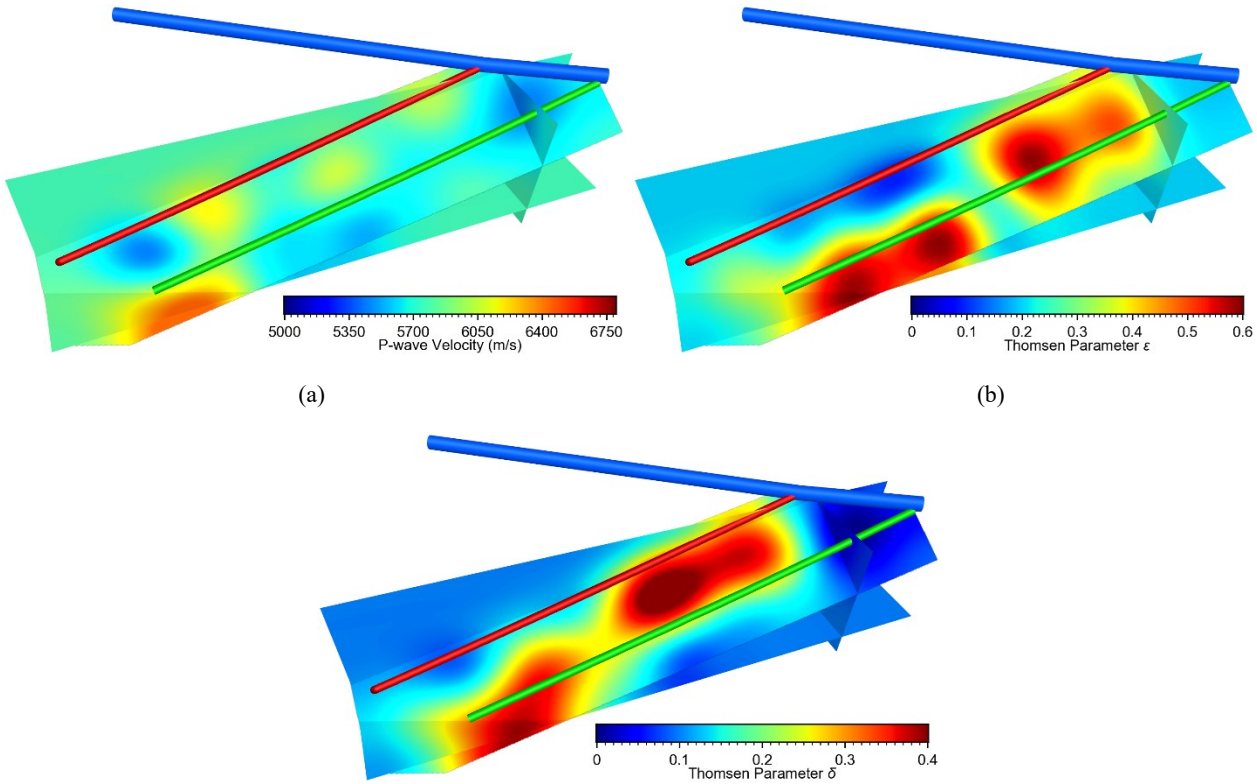

Figure 4: Inverted P-wave velocity (a), Thomsen anisotropic parameter ε (b) and Thomsen anisotropic parameter δ (c) obtained using our AA-FATT by assuming HTI medium.

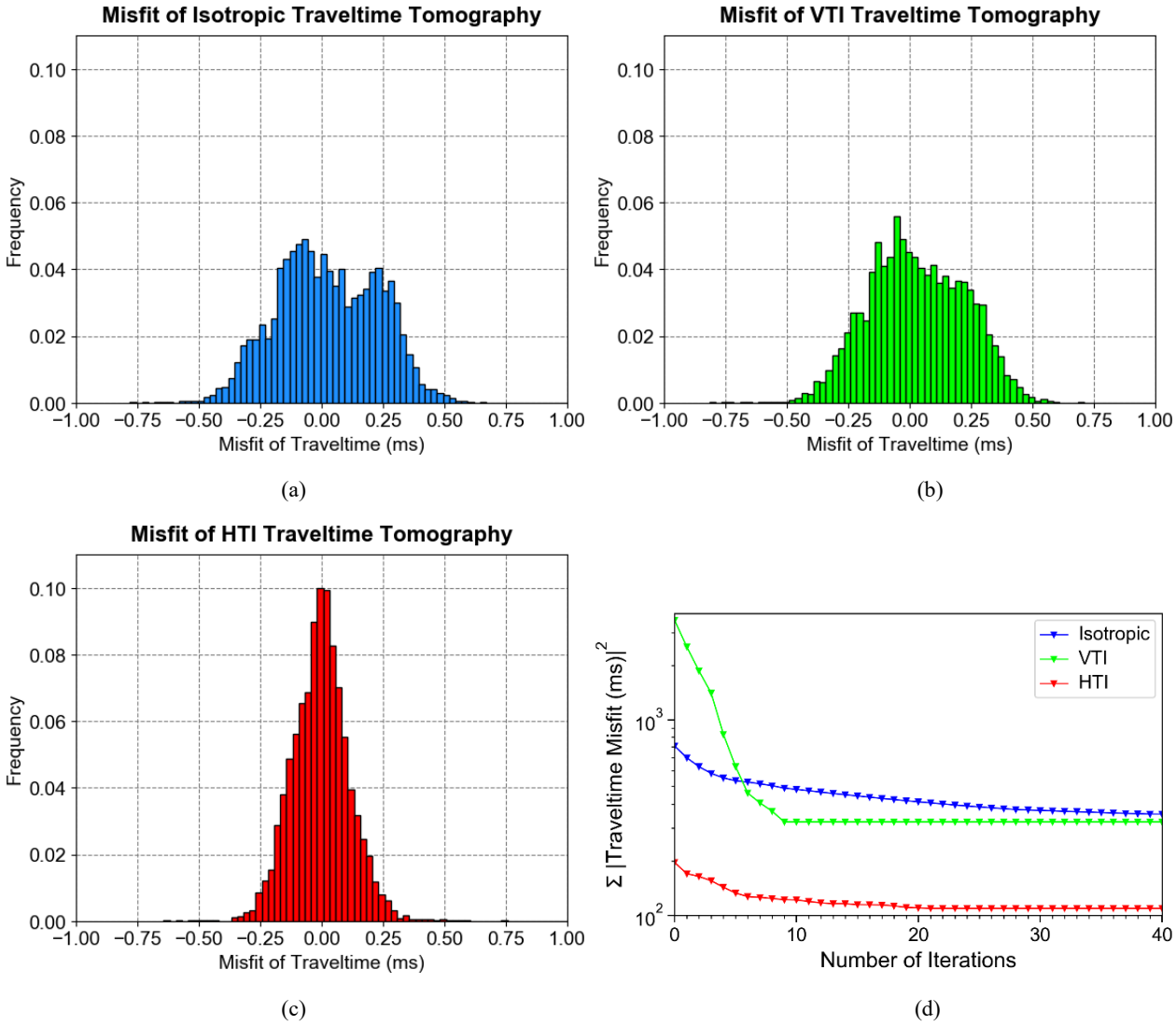

Figure 5: Distributions of traveltime error in the inverted (a) isotropic model, (b) VTI medium model and (c) HTI medium model. Panel (d) compares the traveltime misfit convergence in these three different media.

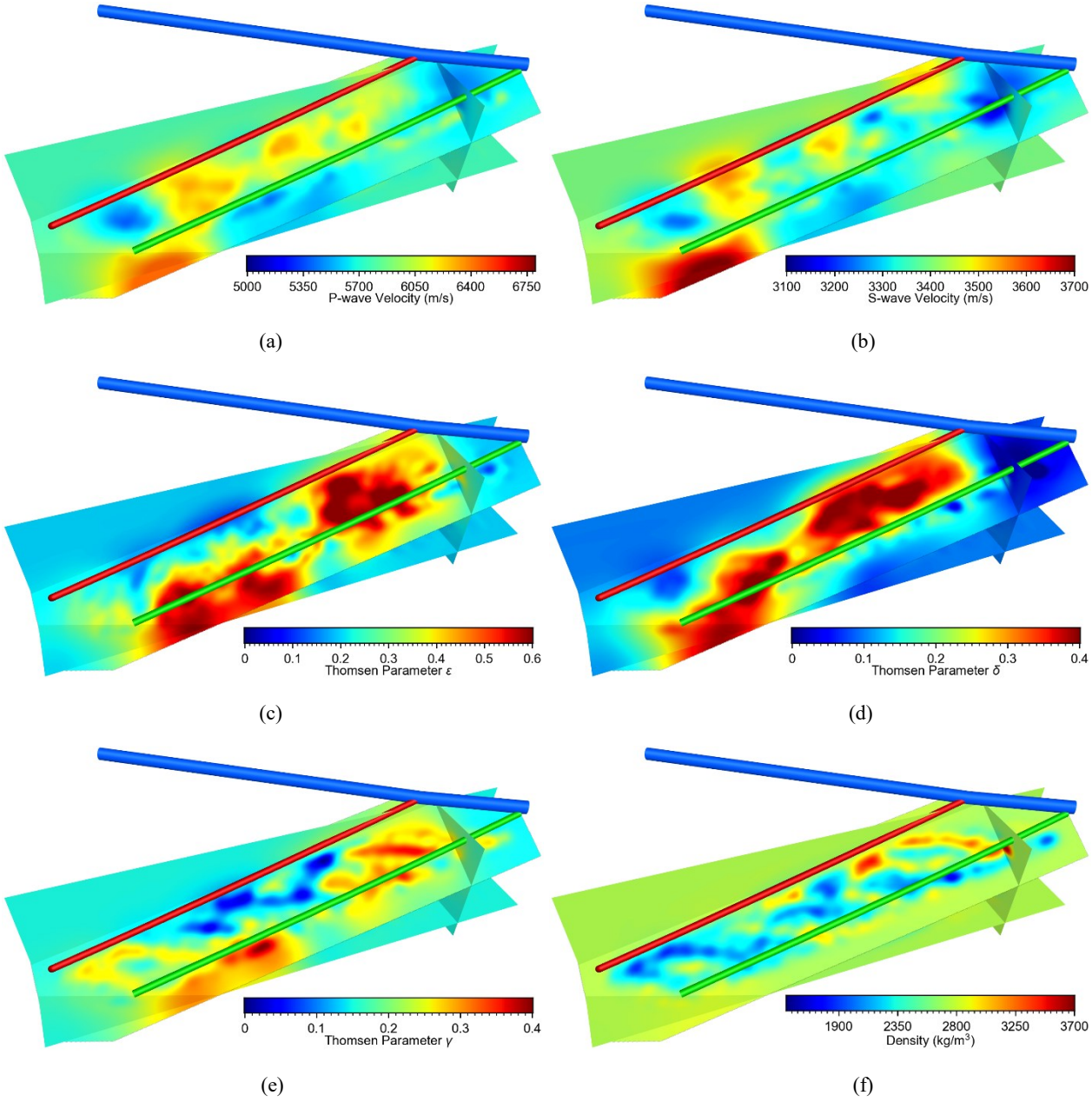

Figure 6: Anisotropic elastic parameter models produced using our 3D AEWI of the campaign cross-borehole seismic data. Panels (a)-(f) show the inverted P-wave velocity, S-wave velocity, Thomsen parameters ε, δ and γ, and density models, respectively. The initial models for AEWI are those shown in Figure 5.

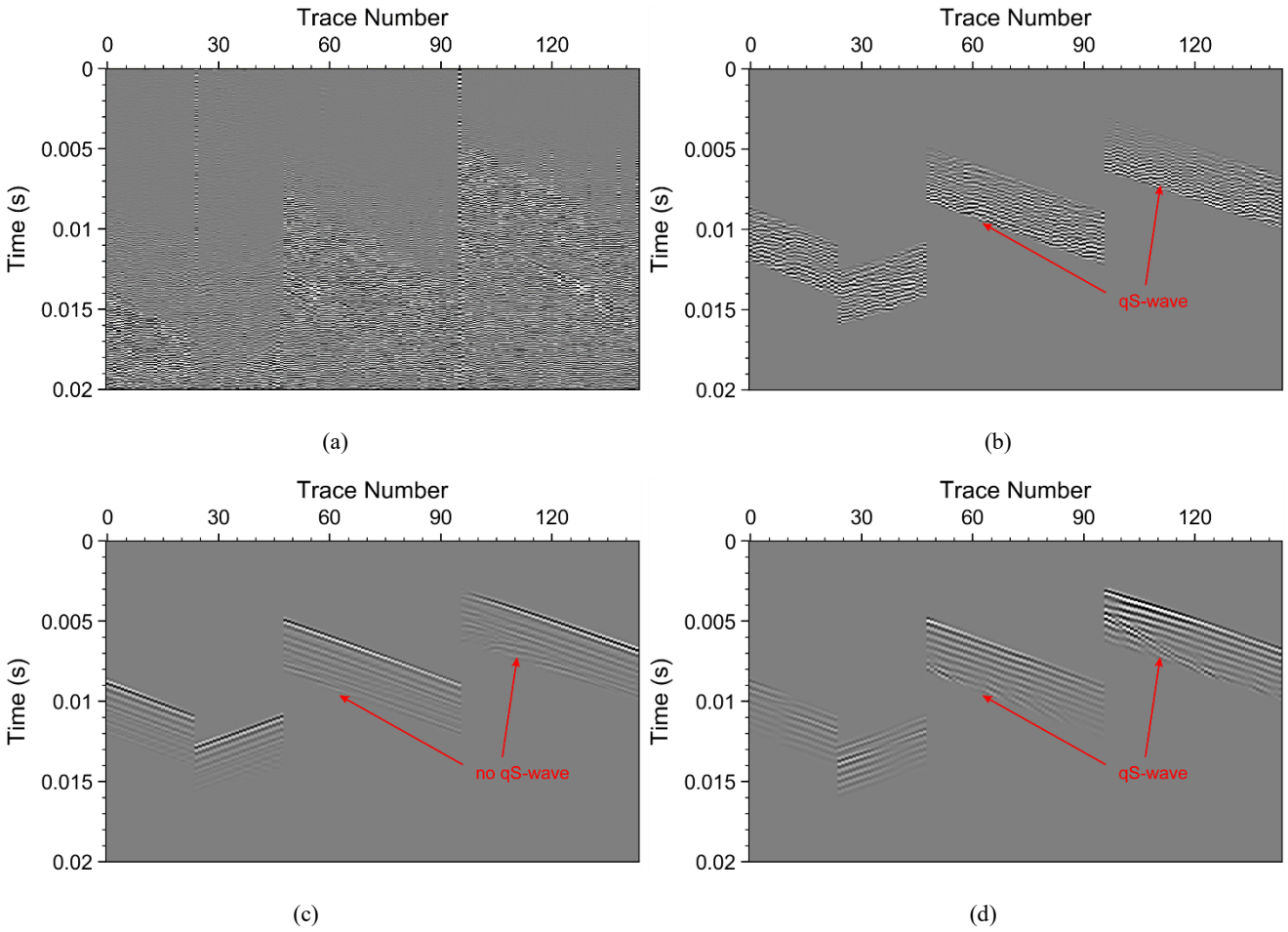

Figure 7: (a) A common-shot gather (pressure component) obtained at the hydrophones in the production well. (b) Processed common-shot gather in (a) as the input for our 3D AEWI. Note the leaked S-wave mode in the pressure component. The S-wave mode has distinct slope compared with the P-wave arrival. (c) The common-gather simulated using 3D elastic-wave equation solver in isotropic medium. There is no visible S-wave mode in the pressure component. (d) The synthetic common-shot gather in the inverted anisotropic elastic model shown in Figure 6. Note the clear evidence of S-wave mode in the pressure component.

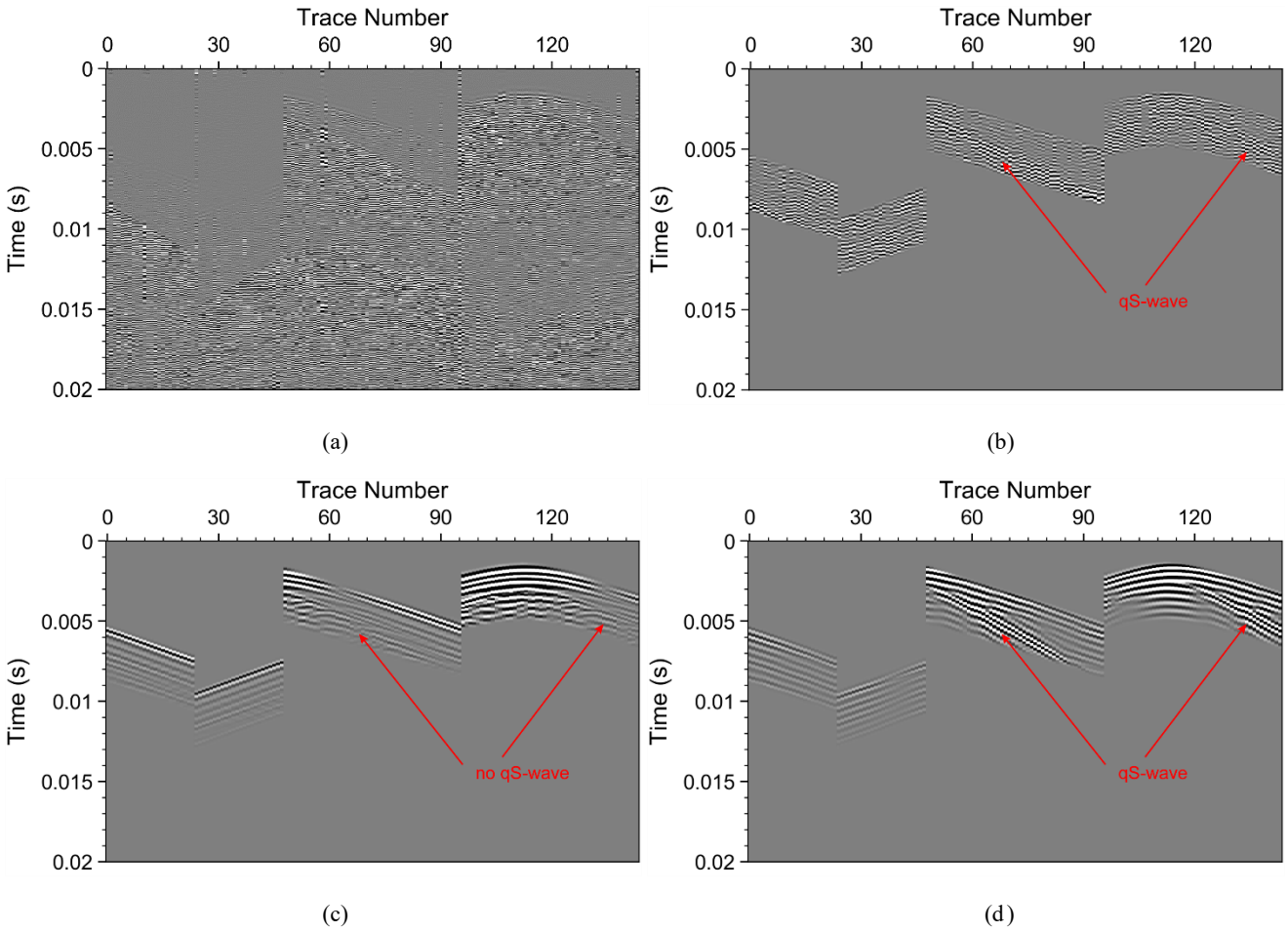

Figure 8: (a) A common-shot gather (pressure component) obtained at the hydrophones in the production well. (b) Processed common-shot gather in (a) as the input for our 3D AEWI. Note the leaked S-wave mode in the pressure component. The S-wave mode has distinct slope compared with the P-wave arrival. (c) The common-gather simulated using 3D elastic-wave equation solver in isotropic medium. There is no visible S-wave mode in the pressure component. (d) The synthetic common-shot gather in the inverted anisotropic elastic model shown in Figure 6. Note the clear evidence of S-wave mode in the pressure component.